nature chemistry

ARTICLES

PUBLISHED ONLINE: 25 JANUARY 2016 | DOI: 10.1038/NCHEM.2438

Reversible Bergman cyclization by atomic manipulation

Bruno Schuler[1], Shadi Fatayer[1], Fabian Mohn[1†], Nikolaj Moll[1], Niko Pavliček[1], Gerhard Meyer[1], Diego Peña[2] and Leo Gross[1*]

The Bergman cyclization is one of the most fascinating rearrangements in chemistry, with important implications in organic synthesis and pharmacology. Here we demonstrate a reversible Bergman cyclization for the first time. We induced the on-surface transformation of an individual aromatic diradical into a highly strained ten-membered diyne using atomic manipulation and verified the products by non-contact atomic force microscopy with atomic resolution. The diyne and diradical were stabilized by using an ultrathin NaCl film as the substrate, and the diyne could be transformed back into the diradical. Importantly, the diradical and the diyne exhibit different reactivity, electronic, magnetic and optical properties associated with the changes in the bond topology, and spin multiplicity. With this reversible, triggered Bergman cyclization we demonstrated switching on demand between the two reactive intermediates by means of selective C–C bond formation or cleavage, which opens up the field of radical chemistry for on-surface reactions by atomic manipulation.

In a pioneering work from 1972[1], Jones and Bergman explained the thermal isomerization of the deuterated enediynes **1** and **3** by proposing a rearrangement reaction through the diradical **2** (1,4-didehydrobenzene or *para*-benzyne), the so-called Bergman cyclization[2] (Fig. 1a). The importance of this reaction was recognized when enediyne anticancer antibiotics were discovered in the late 1980s[3,4]. In particular, these molecules are thought to cleave the double-stranded DNA by a mechanism of action based on the generation and subsequent reaction of 1,4-diradicals[5]. Remarkably, the enediyne moiety in these anticancer drugs is embedded in a nine- or ten-membered ring, which favours the cyclization reaction. In this respect, Bergman cyclizations of strained cyclic diynes have been widely studied. For example, Masamune and co-workers attempted to synthesize the highly reactive diyne **4** in solution, which resulted in the isolation of anthracene[6]. Afterwards, several groups described the spectroscopic characterization of the transient diyne **4**[7–9], and Sander and co-workers reported its matrix isolation[10].

In recent years, on-surface synthesis has been applied successfully to prepare diverse nanostructures using bottom-up approaches[11,12]. Among the reactions employed for this purpose, the Ullmann coupling of halogenated aromatic compounds has emerged as the most successful on-surface chemical transformation[13–16]. In most cases, this reaction is thought to proceed via the dehalogenation of aryl halides followed by C–C coupling of the resulting aryl radicals. Moreover, Bergman cyclizations have also been proposed to play a role in the on-surface synthesis of polyphenylene chains[17] and in the cyclization of oligo-(phenylene-1,2-ethynylenes)[18].

Scanning tunnelling microscopy (STM) made it possible to trigger and image reactions at the level of individual molecules[13,19–25]. The direct visualization of the chemical structure with atomic force microscopy (AFM) using functionalized tips[26] has been used to observe bond making and breaking in a metal–molecule complex[27], to investigate the molecular structure of reactive intermediates formed by atomic manipulation[28] and to identify products formed by on-surface chemistry[18,29].

In this study, a highly strained diyne with a ten-membered ring (**4**) was generated by a sequence of single-molecule reactions that involved two reaction intermediates from 9,10-dibromoanthracene (DBA, **6**) on a bilayer NaCl film on Cu(111). First, DBA was debrominated selectively, one Br at a time, to form the didehydroanthracene diradical **5** and, subsequently, a ring-opening retro-Bergman cyclization was initiated, all by means of atomic manipulation. The structures of the reaction product and intermediates were identified and characterized using AFM. We demonstrate the reversible conversion between the diradical and the diyne, which realizes a tri-state single-molecular switch based on the forward and backward Bergman reaction[1,2] (Fig. 1b).

Results and discussion

We deposited DBA on a Cu(111) surface partly covered by NaCl islands that mainly had a thickness of two monolayers, denoted as

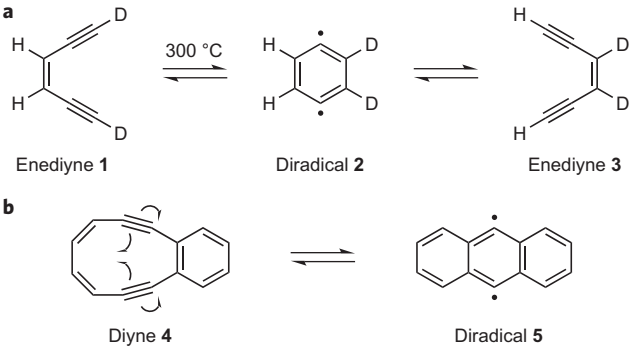

Figure 1 | Bergman cyclizations. a, The seminal experiment[1] regarding the thermal isomerization of deuterated enediynes **1** and **3** through the formation of the diradical [2,3-D_2]-1,4-didehydrobenzene (**2**). **b**, Bergman cyclization of the cyclic diyne 3,4-benzocyclodeca-3,7,9-triene-1,5-diyne (**4**) to generate the 9,10-didehydroanthracene diradical **5**.

[1]IBM Research – Zurich, 8803 Rüschlikon, Switzerland. [2]CIQUS, Universidade de Santiago de Compostela, 15782 Santiago de Compostela, Spain. †Present address: ABB Corporate Research, 5405 Baden-Dättwil, Switzerland. *e-mail: lgr@zurich.ibm.com

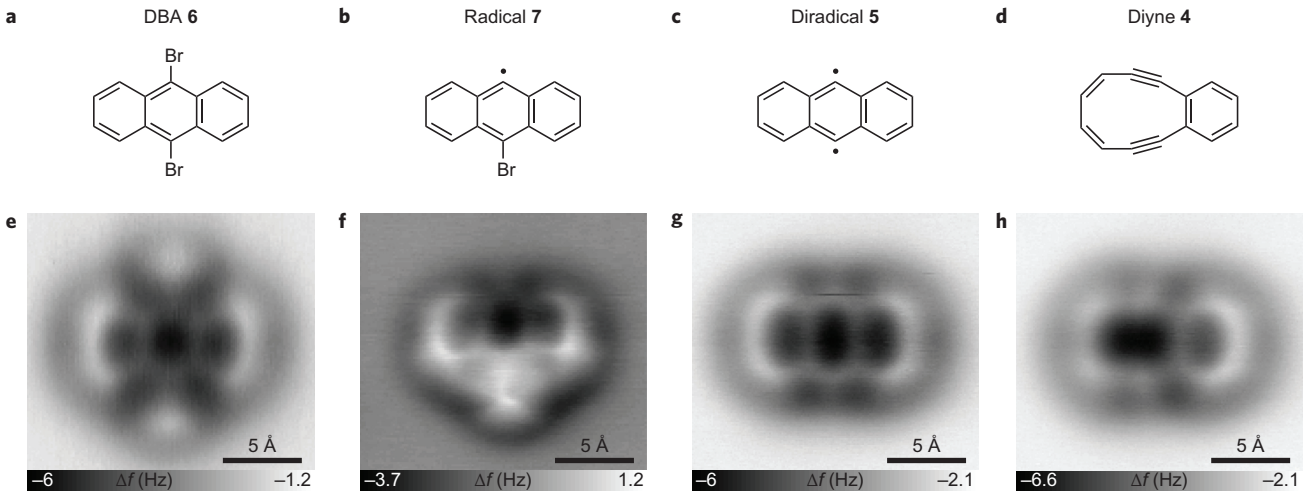

Figure 2 | Structures and AFM imaging of the starting material, reaction intermediates and product. a–d, Chemical structures of the reaction products formed by successive STM-induced debromination of DBA (**6**) (**a**) and subsequent retro-Bergman cyclization: DBA, 9-dehydro-10-bromoanthracene (radical **7**) (**b**), 9,10-didehydroanthracene (diradical **5**) (**c**) and 3,4-benzocyclodeca-3,7,9-triene-1,5-diyne (diyne **4**) (**d**). **e–h**, Corresponding constant-height AFM images of the molecules in **a–d**, respectively, on NaCl(2ML)/Cu(111) using a CO tip. Δf corresponds to the frequency shift of the oscillating cantilever.

NaCl(2ML)/Cu(111). Deposition of molecules with a submonolayer coverage at a sample temperature of approximately 10 K led to individual DBA molecules adsorbed on the surface. We used AFM imaging with CO tips[26] to resolve the chemical structure of the precursor (Fig. 2a) and to identify the intermediates (Fig. 2b,c) and the reaction product (Fig. 2d).

As seen in Fig. 2e, the Br atoms of DBA appear as bright lobes of an increased frequency shift. We dissociated the Br atoms on NaCl (2ML)/Cu(111) by placing the tip above the molecule and applying a voltage pulse. The voltage threshold to dissociate the first Br atom, which forms 9-dehydro-10-bromoanthracene (radical **7**), is about 1.6 V. In the AFM image of the bromoanthryl radical, shown in Fig. 2f, the bright feature that corresponds to the Br atom can only be seen on one side of the molecule. The contrast of the molecule indicates that its adsorption is non-planar with a reduced adsorption height on the debrominated side of the molecule[30,31].

The second C–Br bond was cleaved by applying a voltage pulse of about 3.3 V to form diradical **5**; the tip was retracted by several Ångströms to limit the current to tens of picoamperes. The dissociation processes of both Br atoms were often accompanied by displacements of the organic fragment and these atoms[32]. An AFM image of the diradical is shown in Fig. 2g. As demonstrated for *ortho*-arynes, the NaCl film facilitates the stabilization of reactive intermediates such as radicals and diradicals[28]. Next, a voltage pulse of 1.7 V was applied with the tip above the diradical. AFM imaging of the resulting product, shown in Fig. 2h, revealed a molecule that apparently consisted of fused six- and ten-membered rings, which suggests the formation of diyne **4** by homolytic cleavage of the C–C bond shared by two fused benzene rings. This diyne was often created directly from radical **7** without first observing diradical **5**.

To prove that we had created the cyclic diyne, we employed a combination of STM for orbital imaging[33] (Fig. 3a) and CO-tip AFM images at different tip heights (Fig. 3b–d) and compared the experiments with density functional theory (DFT) calculations (Fig. 3e–h). With orbital imaging, only the negative ion resonance, which corresponds to the lowest unoccupied molecular orbital (LUMO), was in the experimentally accessible voltage range without switching or displacing the molecule. The relative orbital intensities and the location of the nodal planes are in good agreement with the calculated LUMO of the diyne (Fig. 3e), which corroborates our assignment.

The experimental and calculated AFM images of the ten-membered carbon ring of the diyne exhibit features that relate to different bond orders[34] and that lead to a characteristic fingerprint of this moiety. For example, the triple bonds of the structure in Fig. 2d appear with a distinctive elongation perpendicular to the bond direction, as previously found for alkynes imaged by CO tips[18,35]. A detailed bond-order analysis of the diyne and the diradical is given in the Supplementary Information. Also, the benzene ring appears more pronounced in both the measurement and calculation as a result of a small upward bending of the ring. On the metal the diradical could be generated, but no diyne creation was observed, which emphasizes the importance of the insulating layer to stabilize the reactive intermediates[28] and to facilitate the reaction. Instead, the diradical binds to the substrate at the centre of the molecule on Cu(111) (Supplementary Fig. 1). The direct visualization of the molecular structures by AFM and the good agreement of the theoretical calculations with AFM and STM images prove the creation of the diyne and thus the successful execution of a retro-Bergman cyclization using atomic manipulation.

Next, we study the Bergman cyclization reaction in more detail and demonstrate its reversibility and the interconversion between the two possible diyne topomers: diyne **4R**, with the ten-membered ring on the right hand side, and diyne **4L**, with this ring on the left (Fig. 4). Which topomer is created depends on which of the two C–C bonds shared by the fused benzene rings is cleaved. To avoid displacements of the molecule accompanied with switching, we stabilized the diradical at a step edge of a three-layer NaCl island. To this end, we first manipulated the molecule by inelastic excitation[36] to bring it to the NaCl step edge shown in Fig. 4. The bright features seen in the bottom part of Fig. 4a–c correspond to the Cl ions in the third NaCl layer[37]. In the current trace recorded during such switching at 1.64 V (Fig. 4d), we observe switching between three distinct current levels. This voltage corresponds to the onset of the negative-ion resonance of diyne **4** (Fig. 3a). By reducing the voltage to 0 V after switching of the molecule and taking an AFM image, we can relate the three different current plateaus in Fig. 4d to the molecular structures shown in Fig. 4a–c. Figure 4a shows diyne **4R** and corresponds to the low-current state in Fig. 4d. Figure 4b shows the diradical that corresponds to the medium-current state and Fig. 4c shows diyne **4L**, which corresponds to the high-current state in Fig. 4d. The lateral tip position determines the value of the current plateaus measured above the different

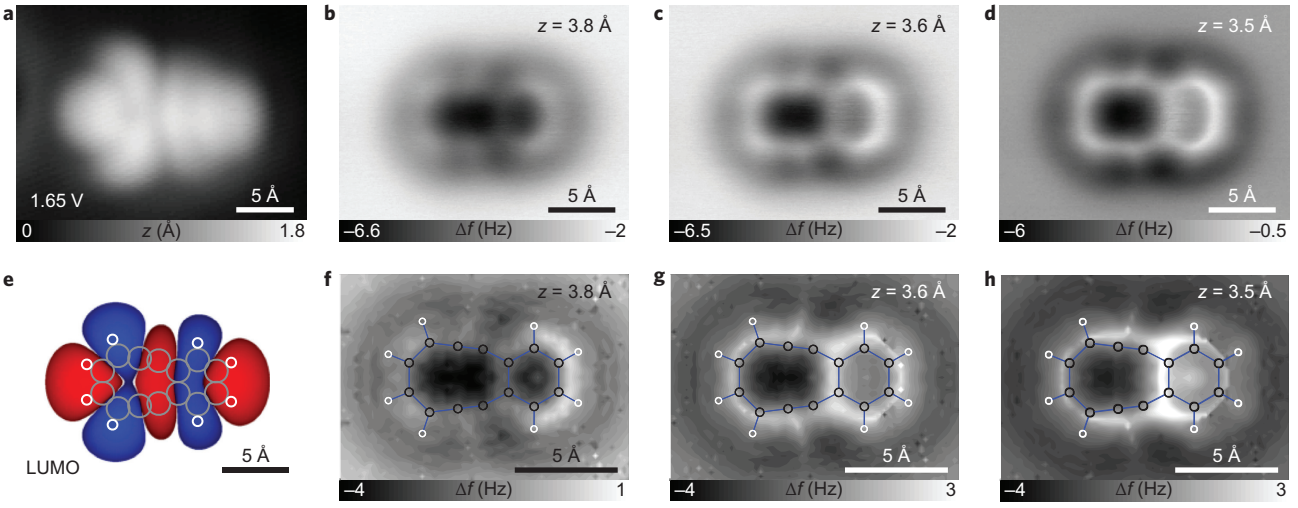

Figure 3 | Diyne identification. a, Constant-current STM image (I = 2 pA, V = 1.65 V) of diyne **4**. **b**–**d**, Constant-height AFM images of diyne **4** on NaCl (2ML)/Cu(111) at different heights z. **e**, Calculated LUMO orbital of diyne **4** with the molecular structure overlaid as a guide to the eye. **f**–**h**, Calculated Δf maps of diyne **4** interacting with a CO tip at tip–molecule distances that correspond to the estimated experimental distances in **b**–**d**.

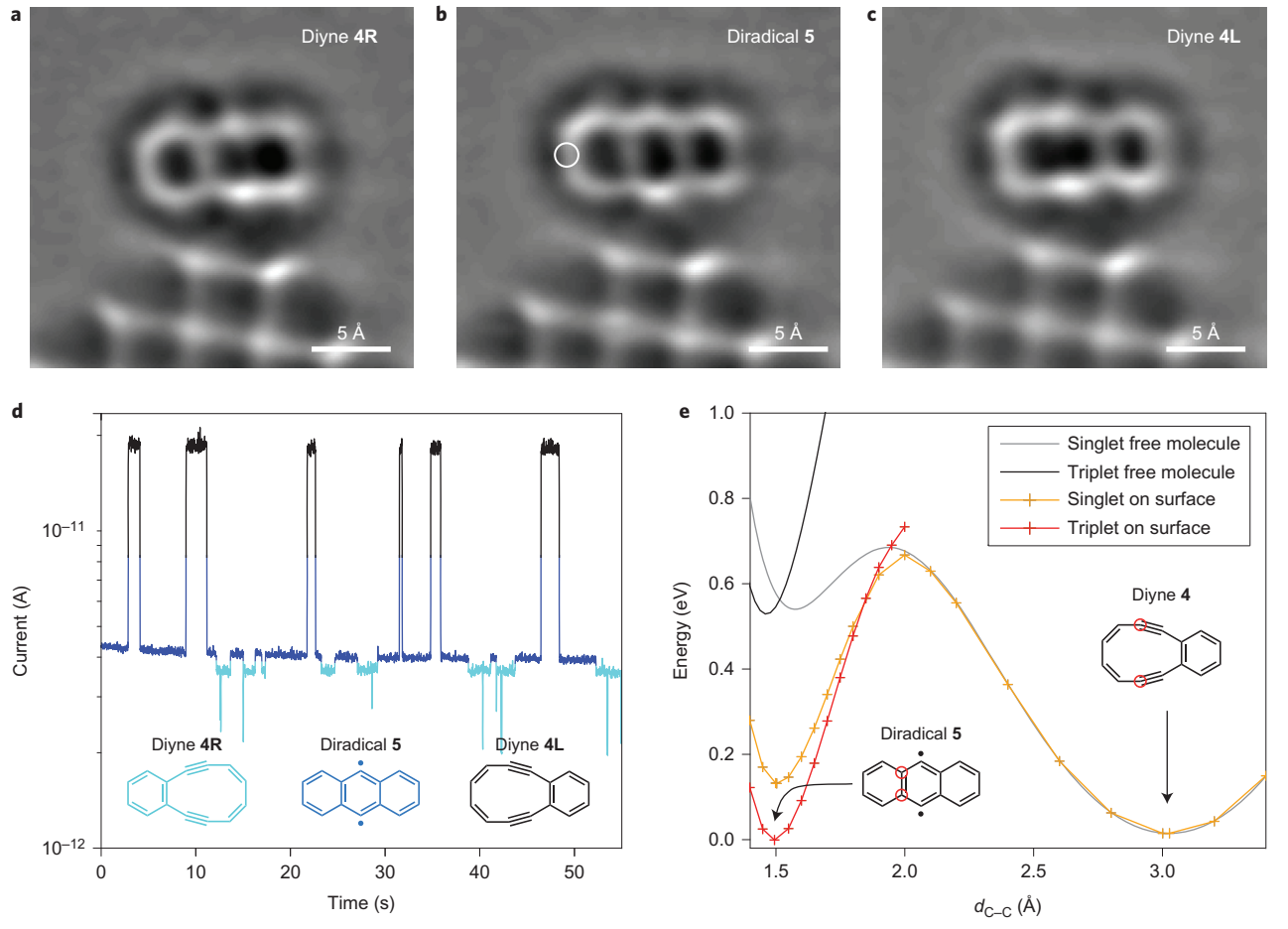

Figure 4 | Reversible Bergman cyclization. a–**c**, Laplace-filtered AFM images of diyne **4R** (**a**), diradical **5** (**b**) and diyne **4L** (**c**) on NaCl(2ML)/Cu(111). The molecule is adsorbed at a step edge of an NaCl(3ML)/Cu(111) island, seen in the lower part of the images. **d**, Current trace during a voltage pulse of V = 1.64 V at the position indicated by the white circle in **b**. The different current levels correspond to the molecular structures of the same colour shown in the inset. **e**, Calculated energies of the Bergman cyclization using the distance between the carbons indicated by red circles (d_{C-C}) as the reaction coordinate.

isomers. As indicated by the white circle in Fig. 4b, we chose an off-centred position to distinguish diyne **4L** from diyne **4R**. The voltage threshold for the Bergman cyclization to take place is close to the LUMO orbital energy of the diyne molecule, which suggests that the process is initiated by an electron attachment. A field-induced process can be excluded as we did not observe a pronounced

distance dependence. The switching yield per electron depends on the environment, in particular on the adsorption at the step-edge that breaks the symmetry of the molecule. The switching trace in Fig. 4d indicates that there is no direct transition between the two different diyne topomers. However, the topomer interconversion always involves the diradical as an intermediate.

These observations demonstrate that the Bergman reaction can be performed reversibly in this system, that is, the two C–C bonds shared by two fused benzene rings within the molecule can be created and cleaved again. We cannot direct in which state the molecule will switch, but we can stop the switching in any of the three molecular states at will. When the voltage was reduced below the reaction threshold, all three molecular structures remained stable and no switching was observed, which enabled the recording of AFM images at a low voltage.

DFT was used to calculate the potential-energy surface of the Bergman cyclization of the free molecule (Fig. 4e, grey and black curves) and the molecule adsorbed on NaCl/Cu(111) (Fig. 4e, orange and red curves), with the carbon–carbon distance of the bond formed during the Bergman reaction as the reaction coordinate. In particular, the effect of spin multiplicity (singlet or triplet) is studied by spin-polarized energy minimization. For both the free molecule and the molecule adsorbed on the surface, the diradical and the diyne form two (meta)stable states. In vacuum, the diyne has a lower absolute energy, by 0.51 eV, compared with that of the diradical, and a barrier of 0.67 eV, which are similar to the values reported previously[10]. Interestingly, in the diradical structure, the triplet state is slightly preferred over the singlet state. On the surface, the diradical energy is significantly lower for both the singlet and triplet states. Consequently, the diradical triplet and the diyne singlet now have approximately the same energy. Additionally, the singlet–triplet splitting of the diradical, 0.15 eV on the surface, is increased compared with that in a vacuum. The comparable energy of the diradical and diyne on the surface and the substantial energy barrier that separates the two states allow us to stabilize both states individually in experiments.

Conclusions

We have demonstrated the sequential on-surface synthesis of a strained diyne by three consecutive single-molecule reactions, starting from DBA, by means of atomic manipulation. The reaction intermediates and products were identified unambiguously and were characterized by atomic-resolution AFM measurements, STM orbital imaging and DFT calculations. The diradical–diyne conversion represents a retro-Bergman cyclization that can be triggered reversibly and involves two diyne topomers that constitute a tri-state molecular switch. Interestingly, the *para*-coupled aromatic diradical has a triplet ground state, which makes this system of potential use as a switchable single-molecule magnet controlled by its molecular structure.

Methods

Experimental details

Set-up. The experiments were performed using a home-built low-temperature ($T \approx 5$ K) ultrahigh vacuum (UVH, $p \approx 10^{-10}$ mbar) combined STM and AFM. The sensor was based on a qPlus[38] quartz-crystal cantilever design operated in the frequency-modulation mode[39] (resonance frequency $f_0 \approx 30$ kHz, spring constant $k \approx 1{,}800$ N m^{-1}, quality factor $Q \approx 14{,}000$ and oscillation amplitude $A \approx 0.5$ Å). The voltage was applied to the sample. STM images were taken in the constant-current mode. AFM measurements were acquired in constant-height mode at $V = 0$ V. The experimental tip height was related to the tip–molecule distance by setting the tip height at the $\Delta f(z)$ minimum above the six-membered carbon ring to $z = 3.9$ Å (ref. 34).

Sample preparation. First, a Cu(111) single crystal was cleaned by repeated sputtering (Ne^+) and annealing (900 K) cycles. Subsequently, NaCl was evaporated at about 270 K, such that (100)-oriented NaCl islands, mostly two atomic layers in thickness, were formed. For the tip preparation, a low coverage (approximately 0.01 nm^{-2}) of CO was deposited on the surface (at $T \approx 10$ K) by admitting CO into the UHV chamber. The DBA molecules were sublimed by flash heating the solid compound from a piece of Si wafer onto the sample (at $T \approx 10$ K).

Tip preparation. For the microscope tip we used a PtIr wire of thickness 25 µm, sharpened with a focused ion beam. Thereafter, we prepared a clean and sharp Cu tip by repeated indentations into the Cu surface. A CO tip was created by picking up a single CO molecule from the surface[26,32]. Apparent distortions of the molecular structure in AFM images result from the CO tilting at the tip[34,40,41].

DFT calculations. The adsorption geometries of the diradical and diyne molecules on a bilayer NaCl film on Cu(100) were calculated with DFT (ref. 42). The Cu(100) surface was used for the calculations because NaCl is commensurate for this surface orientation, which leads to smaller super cells. A code with numerical atomic orbitals as the basis functions[43] and the Perdew–Burke–Ernzerhof exchange-correlation functional[44] was applied. A van der Waals method[45] combined with the Lifshitz–Zaremba–Kohn theory for the non-local Coulomb screening within the bulk for the Cu substrate[46] and calculated coefficients for atoms in the solid[47] for the NaCl film were used. The energy of the triplet state was calculated by performing spin-polarized energy minimization with the spin of the entire unit cell constrained to a spin multiplicity of three. The slab to model the NaCl surface consisted of four layers of Cu substrate with a (001) surface with two layers of NaCl film on top. The (x, y, z) dimension of the calculated cell was (23.10, 15.40, 29.04 Å). The NaCl layers and the two topmost Cu layers were fully relaxed.

We found that in the calculations both the diradical and diyne molecules adsorb with their long axis along a row of Cl atoms in the [011] direction (in agreement with the experiments). For the diradical, the two outer benzene rings are bent downward, so that the outermost C atoms were 0.1 Å closer to the substrate than the inner ones. The diyne ten-membered ring bent downward, so that the outermost C atoms were 0.14 Å closer to the substrate than in the six-membered ring.

We calculated the Bergman cyclization energies by taking the C–C bond length d_{C-C} as the reaction coordinate and fixing it to different values. The frequency-shift spectra were calculated without the underlying substrate, but keeping the atomic positions of the two molecules fixed as found in the adsorption geometry calculated on the substrate. Otherwise, the computational time would be prohibitively long. We calculated the total energy of the molecules that interacted with a vertical Cu-dimer tip functionalized with CO (ref. 34). We used the Cu dimer as the metallic part of the tip in our calculations, because it shows spherical symmetry, and the small number of atoms reduces the computational costs. By changing the length of the Cu dimer the spring constant can be tuned between 0.9 and 0 N m^{-1}. Here we used a dimer length of 2.75 Å, which gives a very small intrinsic spring constant of 0.03 N m^{-1}. The vertical attractive forces, however, lead to an additional position-dependent spring constant of up to 0.26 N m^{-1}. To obtain the frequency shift we took the second derivative with respect to the z direction.

Received 20 August 2015; accepted 11 December 2015; published online 25 January 2016

References

1. Jones, R. R. & Bergman, R. G. *p*-Benzyne. Generation as an intermediate in a thermal isomerization reaction and trapping evidence for the 1,4-benzenediyl structure. *J. Am. Chem. Soc.* **94,** 660–661 (1972).
2. Wenk, H. H., Winkler, M. & Sander, W. One century of aryne chemistry. *Angew. Chem. Int. Ed.* **42,** 502–528 (2003).
3. Nicolaou, K. C., Dai, W.-M., Tsay, S.-C., Estevez, V. A. & Wrasidlo, W. Designed enediynes: a new class of DNA-cleaving molecules with potent and selective anticancer activity. *Science* **256,** 1172–1178 (1992).
4. Nicolaou, K., Smith, A. & Yue, E. Chemistry and biology of natural and designed enediynes. *Proc. Natl Acad. Sci. USA* **90,** 5881–5888 (1993).
5. Sinha, S. C. *et al.* Prodrugs of dynemicin analogs for selective chemotherapy mediated by an aldolase catalytic Ab. *Proc. Natl Acad. Sci. USA* **101,** 3095–3099 (2004).
6. Darby, N. *et al.* Concerning the 1,5-didehydro-[10]-annulene system. *J. Chem. Soc. D* **23,** 1516–1517 (1971).
7. Chapman, O., Chang, C. & Kolc, J. 9,10-Dehydroanthracene. A derivative of 1,4-dehydrobenzene. *J. Am. Chem. Soc.* **98,** 5703–5705 (1976).
8. Schottelius, M. J. & Chen, P. 9,10-Dehydroanthracene: *p*-benzyne-type biradicals abstract hydrogen unusually slowly. *J. Am. Chem. Soc.* **118,** 4896–4903 (1996).
9. Wenk, H. H. & Sander, W. Photochemistry of 9,10-dicarbonyl-9,10-dihydroanthracene—a source of 9,10-dehydroanthracene? *Eur. J. Org. Chem.* **1999,** 57–60 (1999).
10. Kötting, C., Sander, W., Kammermeier, S. & Herges, R. Matrix isolation of 3,4-benzocyclodeca-3,7,9-triene-1,5-diyne. *Eur. J. Org. Chem.* **1998,** 799–803 (1998).
11. Perepichka, D. F. & Rosei, F. Extending polymer conjugation into the second dimension. *Science* **323,** 216–217 (2009).
12. Palma, C.-A. & Samorì, P. Blueprinting macromolecular electronics. *Nature Chem.* **3,** 431–436 (2011).
13. Hla, S.-W., Bartels, L., Meyer, G. & Rieder, K.-H. Inducing all steps of a chemical reaction with the scanning tunneling microscope tip: towards single molecule engineering. *Phys. Rev. Lett.* **85,** 2777–2780 (2000).

14. Grill, L. *et al.* Nano-architectures by covalent assembly of molecular building blocks. *Nature Nanotech.* **2,** 687–691 (2007).
15. Cai, J. *et al.* Atomically precise bottom-up fabrication of graphene nanoribbons. *Nature* **466,** 470–473 (2010).
16. Lafferentz, L. *et al.* Controlling on-surface polymerization by hierarchical and substrate-directed growth. *Nature Chem.* **4,** 215–220 (2012).
17. Sun, Q. *et al.* On-surface formation of one-dimensional polyphenylene through Bergman cyclization. *J. Am. Chem. Soc.* **135,** 8448–8451 (2013).
18. de Oteyza, D. G. *et al.* Direct imaging of covalent bond structure in single-molecule chemical reactions. *Science* **340,** 1434–1437 (2013).
19. Stipe, B. *et al.* Single-molecule dissociation by tunneling electrons. *Phys. Rev. Lett.* **78,** 4410–4413 (1997).
20. Lee, H. J. & Ho, W. Single-bond formation and characterization with a scanning tunneling microscope. *Science* **286,** 1719–1722 (1999).
21. Zhao, A. *et al.* Controlling the Kondo effect of an adsorbed magnetic ion through its chemical bonding. *Science* **309,** 1542–1544 (2005).
22. Repp, J., Meyer, G., Paavilainen, S., Olsson, F. E. & Persson, M. Imaging bond formation between a gold atom and pentacene on an insulating surface. *Science* **312,** 1196–1199 (2006).
23. Liljeroth, P., Repp, J. & Meyer, G. Current-induced hydrogen tautomerization and conductance switching of naphthalocyanine molecules. *Science* **317,** 1203–1206 (2007).
24. Albrecht, F., Neu, M., Quest, C., Swart, I. & Repp, J. Formation and characterization of a molecule–metal–molecule bridge in real space. *J. Am. Chem. Soc.* **135,** 9200–9203 (2013).
25. Kumagai, T. *et al.* Controlling intramolecular hydrogen transfer in a porphycene molecule with single atoms or molecules located nearby. *Nature Chem.* **6,** 41–46 (2014).
26. Gross, L., Mohn, F., Moll, N., Liljeroth, P. & Meyer, G. The chemical structure of a molecule resolved by atomic force microscopy. *Science* **325,** 1110–1114 (2009).
27. Mohn, F. *et al.* Reversible bond formation in a gold-atom–organic-molecule complex as a molecular switch. *Phys. Rev. Lett.* **105,** 266102 (2010).
28. Pavliček, N. *et al.* On-surface generation and imaging of arynes by atomic force microscopy. *Nature Chem.* **7,** 623–628 (2015).
29. Riss, A. *et al.* Local electronic and chemical structure of oligo-acetylene derivatives formed through radical cyclizations at a surface. *Nano Lett.* **14,** 2251–2255 (2014).
30. Pavliček, N. *et al.* Atomic force microscopy reveals bistable configurations of dibenzo[a,h]thianthrene and their interconversion pathway. *Phys. Rev. Lett.* **108,** 086101 (2012).
31. Schuler, B. *et al.* Adsorption geometry determination of single molecules by atomic force microscopy. *Phys. Rev. Lett.* **111,** 106103 (2013).
32. Mohn, F., Schuler, B., Gross, L. & Meyer, G. Different tips for high-resolution AFM and STM imaging of single molecules. *Appl. Phys. Lett.* **102,** 073109 (2013).
33. Repp, G., Meyer, G., Stojkovic, S. M., Gourdon, A. & Joachim, C. Molecules on insulating films: scanning-tunneling microscopy imaging of individual molecular orbitals. *Phys. Rev. Lett.* **94,** 026803 (2005).
34. Gross, L. *et al.* Bond-order discrimination by atomic force microscopy. *Science* **337,** 1326–1329 (2012).
35. Moll, N. *et al.* Image distortions of partly fluorinated hydrocarbons in atomic force microscopy with carbon monoxide terminated tips. *Nano Lett.* **14,** 6127–6131 (2014).
36. Swart, I., Sonnleitner, T., Niedenführ, J. & Repp, J. Controlled lateral manipulation of molecules on insulating films by STM. *Nano Lett.* **12,** 1070–1074 (2012).
37. Gross, L. *et al.* Organic structure determination using atomic resolution scanning probe microscopy. *Nature Chem.* **2,** 821–825 (2010).
38. Giessibl, F. J. High-speed force sensor for force microscopy and profilometry utilizing a quartz tuning fork. *Appl. Phys. Lett.* **73,** 3956–3958 (1998).
39. Albrecht, T. R., Grütter, P., Horne, D. & Rugar, D. Frequency modulation detection using high-Q cantilevers for enhanced force microscope sensitivity. *J. Appl. Phys.* **69,** 668–673 (1991).
40. Boneschanscher, M. P., Hämäläinen, S. K., Liljeroth, P. & Swart, I. Sample corrugation affects the apparent bond lengths in atomic force microscopy. *ACS Nano* **8,** 3006–3014 (2014).
41. Hapala, P. *et al.* The mechanism of high-resolution STM/AFM imaging with functionalized tips. *Phys. Rev. B* **90,** 085421 (2014).
42. Hohenberg, P. & Kohn, W. Inhomogeneous electron gas. *Phys. Rev.* **136,** B864–B871 (1964).
43. Blum, V. *et al. Ab initio* molecular simulations with numeric atom-centered orbitals. *Comp. Phys. Comm.* **180,** 2175–2196 (2009).
44. Perdew, J. P., Burke, K. & Ernzerhof, M. Generalized gradient approximation made simple. *Phys. Rev. Lett.* **77,** 3865–3868 (1996).
45. Tkatchenko, A. & Scheffler, M. Accurate molecular van der Waals interactions from ground-state electron density and free-atom reference data. *Phys. Rev. Lett.* **102,** 073005 (2009).
46. Ruiz, V. G., Liu, W., Zojer, E., Scheffler, M. & Tkatchenko, A. Density-functional theory with screened van-der-Waals interactions for the modeling of hybrid inorganic–organic systems. *Phys. Rev. Lett.* **108,** 146103 (2012).
47. Zhang, G.-X., Tkatchenko, A., Paier, J., Appel, H. & Scheffler, M. Van der Waals interactions in ionic and semiconductor solids. *Phys. Rev. Lett.* **107,** 245501 (2011).

Acknowledgements

We thank I. Tavernelli, D. Pérez, E. Guitián and R. Allenspach for discussions. We acknowledge financial support from the European Research Council Advanced Grant CEMAS (agreement no. 291194), the European Union project PAMS (610446) and the Initial Training Network's QTea (317485) and ACRITAS (317348) programs. D.P. acknowledges the Spanish Ministry of Science and Competitiveness for financial support (MAT2013-46593-C6-6-P).

Author contributions

B.S., S.F., F.M., N.P., G.M. and L.G. performed the STM/AFM experiments. N.M. performed the DFT calculations. D.P. identified the reaction. All the authors analysed the data and contributed to the manuscript.

Additional information

Supplementary information and chemical compound information are available in the online version of the paper. Reprints and permissions information is available online at www.nature.com/reprints. Correspondence and requests for materials should be addressed to L.G.

Competing financial interests

The authors declare no competing financial interests.